Supporting Information

# Intelligent anti-impact elastomers by precisely tailoring the topology of modular polymer network

*Jianfeng Cheng,[a] Xianhua Yao,[a] Zhipeng Zhang,[b] Yizhong Tan,[c] Nan Hu,[a] Chunfeng Ma*[ab] and Guangzhao Zhang*[ab]*

[a]School of Civil Engineering and Transportation, South China University of Technology, Guangzhou 510640, P. R. China. E-mail: msmcf@scut.edu.cn (CM);

[b]Faculty of Materials Science and Engineering, South China University of Technology, Guangzhou 510640, P. R. China.

[c]National Defense Engineering College, Army Engineering University of PLA, Nanjing 210007, P. R. China.

*E-mail: msmcf@scut.edu.cn (CM);

## Experimental Procedures

### *Materials*

Butyl methacrylate (BMA), isophorone diisocyanate (IPDI), hexamethylene diisocyanate (HDI), dicyclohexylmethane 4,4'-Diisocyanate (HMDI), methyltrimethoxysilane (MTMS), (3-mercaptopropyl)trimethoxysilane (KH590), (3-glycidyloxypropyl)trimethoxysilane (KH560), polyetheramine (D230, D400, and D2000, $M_n$ = 230 g·mol$^{-1}$, 400 g·mol$^{-1}$, and 2,000 g·mol$^{-1}$, respectively) were from Energy-Chemical and used as received. Azobisisobutyronitrile (AIBN) was from Aladdin and purified by recrystallizing in methanol. Hydrogen chloride solution (HCl, 37 wt%), tetrahydrofuran (THF) and ethanol were from Sinopharm and used as received. The Kevlar was from DuPont. PBS gel (D3179), silicone (RTV-4130) were from Dow Corning. Alumina ceramic sheets (96%, 100×100×5 mm$^3$, 100×100×1 mm$^3$, and 100×100×0.5 mm$^3$) were purchased from Guangzhou Baile New Material Co. Ltd. Other common materials like PMMA, PET, PI, NBR were commercially available.

### ***Synthesis of the building blocks in modular polymer network.***

The stereoscopic building blocks (epoxy-oligosiloxane nanoclusters) were prepared by sol–gel reaction. The linear building block (amino-terminated polyurea) was prepard via a polymerization between isocyanates and excess polyetheramine.

**Epoxy-methyl oligosiloxane nanocluster (MC):** In the experimental procedure, MTMS (15.0 g), KH560 (5.0 g), and THF (80.0 g) were introduced into a flask equipped with a magnetic stirrer. Following the initiation of stirring, a solution containing 0.4 g of hydrogen chloride (HCl, 37 wt%) and 4 g of water was added. The

mixture was heated at 75 °C for 10 h, after which it was subjected to vacuum concentration to remove volatile components. The resultant material, referred to as MC, was obtained as a colorless, viscous liquid.

**Epoxy-poly(butyl methacrylate) oligosiloxane nanocluster (BC):** The PBMA was synthesized according to the procedure reported in existing literature.[1] Thereafter, PBMA (39.2 g) and KH560 (13 g) were added to a flask with a magnetic stirrer. 500 mL of ethanol was added as solvent. Moreover, 10 g hydrogen chloride solution (HCl, 37 wt%) was added to the solution after the magnetic stirrer started stirring. The solution was heated at 75 °C for 24 h and then concentrated under vacuum to remove ethanol. The products were extracted by water and trichloromethane, the two types of solution were further separated using a separatory funnel, BC was obtained after removing the trichloromethane.

**Amino-terminated polyurea (APU):** All amino-terminated polyureas were prepared by mixing the isocyanate and polyetheramine. They were mixed with DMF to obtain a 20% solids solution. Polyetheramines solution was first added in a flask and placed in ice water. Then, the isocyanate solution was gradually injected into the flask with a syringe pump at a rate of 300 $\mu L \cdot min^{-1}$. This procedure should ensure that the solution is well-stirred during the injection process. The amino-terminated polyurea was obtained after removing DMF by rotary evaporation.

***Synthesis of IAE***

The IAE was synthesized by simply mixing the ethanol solution of MC, BC, and APU in a flask. Typically, IPU-30BC was prepared by mixing MC (1 g), BC (3 g), and APU

(6.0 g) in ethanol (20 mL); the solution should be sealed and placed for 2 d and poured into a silicone mold and placed for 5 d to slowly evaporate the ethanol. Note that the solution should be placed in a dry environment at approximately 20 °C.

***Preparation of anti-impact composites***

The raw of IAE (MC, BC, APU) were completely mixed for use. To prepare composite fabric, the Kevlar fabric was dipped coating in solution of IAE and placed on a flat surface for 7 d to obtain the composite fabric. For composite ceramics, the solution was dropped in the ceramics and dried for 2 h, the ceramic can be adhered when most of the ethanol in the solution evaporated, and then another ceramic piece is placed on the top. These steps were repeated several times until the composite ceramics with the required number of layers were obtained.

**Characterization**

***Structural characterization.*** 1H NMR and $^{29}Si$ NMR spectra were tested using a Bruker AV600 spectrometer operating at 600 MHz in $CDCl_3$. Fourier Transform Infrared (FTIR) spectra was tested using the KBr press method on Bruker VECTOR-22 FTIR spectrometer in the range of 400–4000 $cm^{-1}$. Gel Permeation Chromatography (GPC) was performed using an Agilent 1260 Infinity instrument, equipped with refractive index and ultraviolet detectors. The analysis was carried out using anhydrous THF as the eluent at 35 °C. The crystalline phase of the samples was determined by PANalytical X-ray diffractometer (XRD) with Cu Kα radiation (λ = 0.15406 nm), scanning from 2−90°. The small-angle X-ray scattering (SAXS) were conducted at Bruker NanoSTAR with a range of 0.074−2.5 nm.

***Particle size for oligosiloxane nanocluster.*** Transmission electron microscope (TEM) was performed using JEM-F200 to determine the specific dimensions and morphological structure of MC and BC. Dynamic light scattering (DLS) was measured using HORIBA SZ-100Z to test the average particle size and size distribution of particles.

***Topographic observation.*** The topography of Kevlar fabric and composite fabric was observed by scanning electron microscope (SEM).

***Thermal analysis test.*** Thermal decomposition process was measured by NETZSCH TG 209F3 in the temperature range of 30−850 °C under $N_2$ atmosphere where the heating rate was 10 °C·min$^{-1}$. Thermal transitions of polymer were observed using Netzsch DSC 200F3. Heating procedure was from −80 to 100 °C, at rate of 10 °C·min$^{-1}$.

***Mechanical tests.*** Tensile and compression properties were all measured using an Instron 5966 instrument at 25 °C. Samples for tensile were dumbbell-shaped with 12 mm length, 2 mm width, and 1 mm thickness. The toughness was calculated by the integration of stress-strain curves. The elastic moduli was calculated through the equation $E = \frac{\Delta\sigma_{5\%} - \Delta\sigma_{2\%}}{\Delta\varepsilon_{5\%} - \Delta\varepsilon_{2\%}}$. For compression test, the sample were square-shaped with 20 mm width and 8 mm thickness. The strain rates were 5 mm·min$^{-1}$, 50 mm·min$^{-1}$, 500 mm·min$^{-1}$ respectively. Dynamic compression was tested by SHPB system. The samples were cylindrical with a diameter of 8 mm and a thickness of 2 mm. The strain rates were from 750 s$^{-1}$ to 24,000 s$^{-1}$.

***Rheology tests.*** The Rheology properties were measured using an Anton Paar MCR-

102 rheometer. The samples had a cylindrical shape with a diameter of 25 mm and a thickness of 1 mm. The frequency rate was varied from 0.1 to 100 Hz and the shear strain was 0.01%. The sample were tested in different temperatures (−15 to 85 °C, ΔT = 10.0 °C, where ΔT describes the temperature interval). The rheological properties of the material at different frequencies are obtained from the WLF equation. In LAOS tests, the sinusoidal alternating stress (20 kPa) at angular rates of 1 Hz were applied to the sample. The hysteresis loop area represented the mechanical energy that converted to heat each cycle, and the energy dissipation was calculated through the circular area.[2]

***Transmittance Tests.*** The UV-vis transmittance spectra were obtained by a UV-vis spectrophotometer (Evolution 220, Thermo Scientific, U. S).

***Dielectric tests.*** The dielectric spectrometer test was performed using α-ANB (Novo-control Technologies, Germany); the size of the sample was 20 mm in diameter and 0.5 mm in thickness. The frequency was from 1 Hz to$10^7$ Hz, and the test temperature was from 0 °C to 40 °C.

***Bending resistance tests.*** The fold-resistance of elastomer was tests by film bending tester. The samples with a thickness of 1 mm was bent to a U shape with an inner diameter of 2 mm and then released. The bending and releasing processes were repeated 10,000 times.

***Adhesion tests.*** The adhesion of elastomer in different substrates were performed by an automatic tester (PosiTest, Model AT-A) according to ASTM D4541-22,[3] the coating surface was polished lightly by abrasive paper Before test. The rate of pull was set to 0.2 MPa·$s^{-1}$. The average adhesion strength was calculated based on 5 different regions

of the coatings.

***Falling ball impact tests.*** The sample was stuck on a holder connected with a mechanical sensor. A steel ball (33 g) freely fell from a height of 20 cm, 40 cm, 60 cm, and 80 cm, hitting the samples with the thicknesses of 1 mm, 2 mm, and 4 mm. Force–time curve was analyzed from the collected data. The frequency signal was 30 kHz.

***Impact resistance tests.*** The drop-hammer impact test was investigated to examined the blunt impact of rigid composites using an Instron 9440.[4] A 6.4 kg hemispherical impactor with a diameter of 10 mm was dropped from different heights to obtain the initial impact velocity $V_{ini}$ of 0.8 m·s$^{-1}$, 1.2 m·s$^{-1}$, and 1.6 m·s$^{-1}$. The impact force $F(t)$ was collected by a force sensor. The displacement U(t) was calculated through the equation $U(t) = \int_0^t V(t)dt$, where, velocity of impactor $V(t)$ was calculated from $V(t) = V_{ini} + \int_0^t \frac{(g - F(t))}{m}dt$, $g$ is the standard gravity. The energy dissipation $E_{dis}$ is the area included inside the loop of the force-displacement curves, and the initial energy $E_{ini}$ was calculated from $E_{ini} = \frac{mV_{ini}}{2}$.

***Puncture tests.*** The drop tower was built to tested the sharp injuries using a needle-shape impactor dropped from 20 cm, 40 cm, 60 cm, 80 cm, and 100 cm height to puncture the composite fabric (Fig. 5f). The acceleration data $a(t)$ was collected by an acceleration sensor. The displacement U(t) was calculated through the equation $U(t) = \iint_0^t a(t)dt$. The corresponding load F was calculated from $F(t) = ma(t) - mg$. The puncture force is the maximum values of load in the force-

displacement.

***Ballistic impact tests.*** The ballistic impact for the bulletproofing experiments of flexible composite fabric was tested according to NIJ Standard 0101.06 and MIL-DTL-46593B.[5–7] A 2 g steel ball was fired through an air gun with a velocity of 250. All edges of fabric were clamped in the experience. The ballistic experiments on rigid composite was immobilized in a heavy-duty steel frame with the four edges of the sample tightly clamped. The air gun was inflated by air compressor to fire 8 g steel balls at 120 $m \cdot s^{-1}$. A high-speed video camera (Phantom) was used to capture the deformation and destruction process and record the projectile position for calculating the residual velocity. The characterizations of these composites in ballistic impact tests were listed in Table S6 and Table S7.

***Finite element simulations.*** Simulations of the impact process was built using the commercial software ANSYS/LS-DYNA. A 2.0 g rigid steel ball with a density of 7.85 $g \cdot cm^{-3}$ impacted the center of a round plain-woven fabric at a speed of 250 $m \cdot s^{-1}$ in the normal direction. The fabric model was created at the yarn cluster-level. The cross-section of the yarn was composed of two identical sine curves facing each other. The thickness was 0.3 mm and the yarn crimp wavelength was 2 mm. Single-point integration element was used to simulate the steel ball and fabric. There was a 0.1 mm thick coating on the surface of the fabric which was simulated by shell element. The explicit dynamics was implemented to characterize the process that a rigid bullets hits composite, and the stress distribution were obtained within 30 μs impact process. Two types of contact settings were: “CONTACT_ERODING_SURFACE_TO_SURFACE”

for eroding between steel and fabric, “CONTACT_TIED_SURFACE_TO_SURFACE” for interfaces between the fabric or coating. The parameters of all materials were shown in Table S8, Table S9, and Table S10, where the mechanical modeling of Kevlar and PBS were adapted from reference.[8,9]

**SI Figures and Tables**

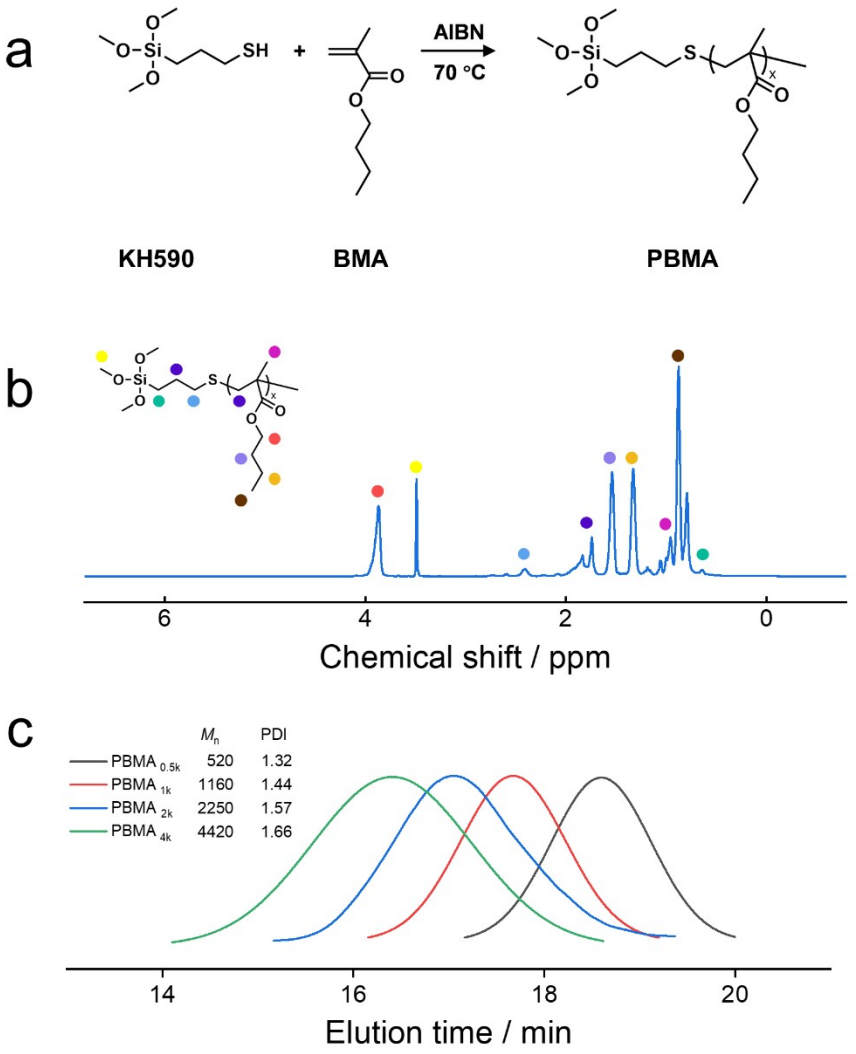


**Fig. S1.** Synthesis and characterization of PBMA. (a) The synthesis of PBMA via telomerization; (b) $^{1}$H NMR spectra of PBMA; (c) The GPC elution curves of PBMA.

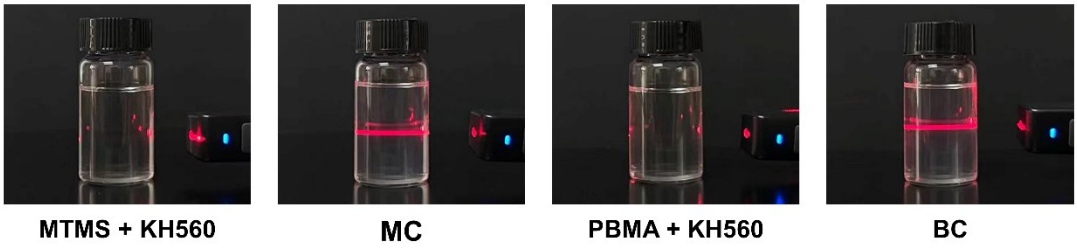


**Fig. S2.** The Tyndall effect of MC and BC. The fact indicates that the MC and BC prepared by sol–gel reaction are nanoclusters with a diameter range of 1–100 nm.

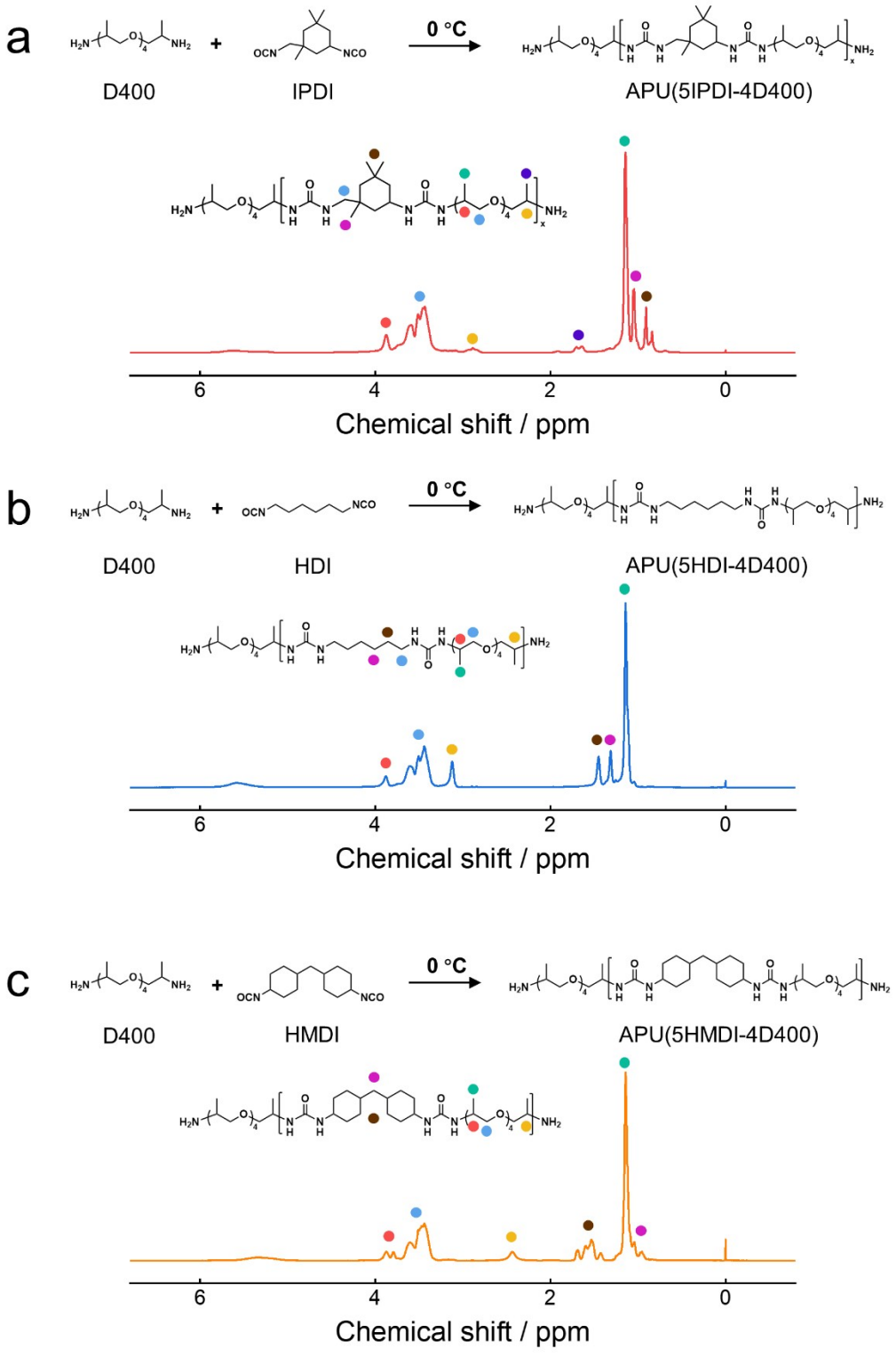


**Fig. S3.** $^{1}$H NMR spectra of polyurea with different isocyanate. (a) IPDI-D400; (b) HDI-D400; (c) HMDI-D400.

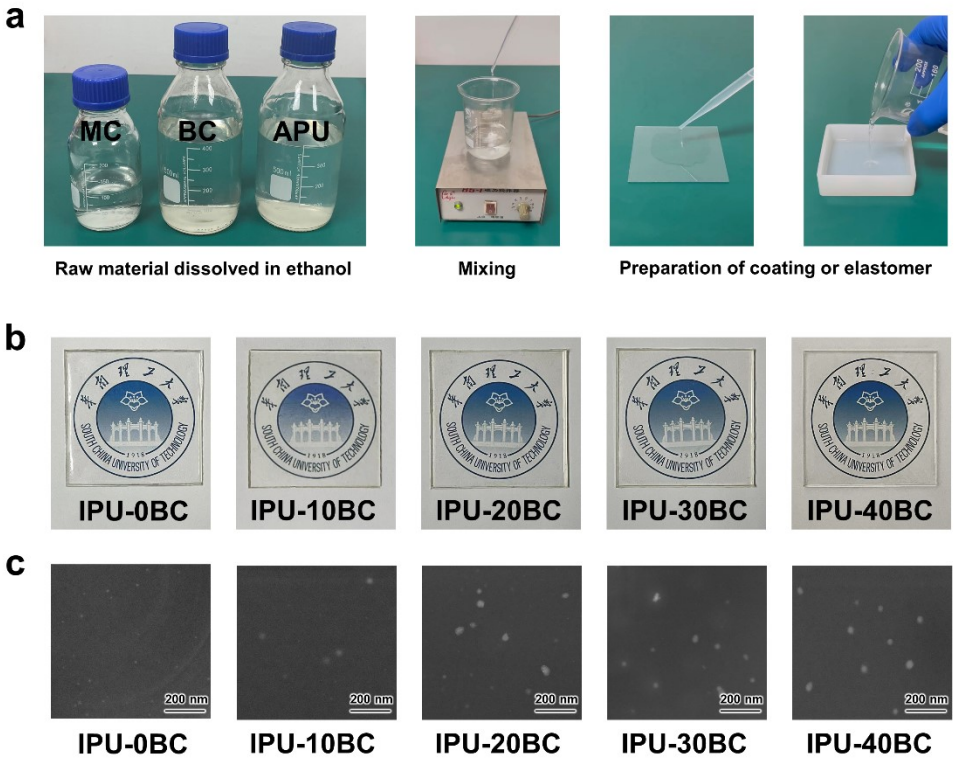


**Fig. S4.** The IAEs with different BC content and their preparation. (a) Preparation process of IAE; (b) Photographs of IAEs. (c) TEM images of nanoclusters in IPU-xBC.

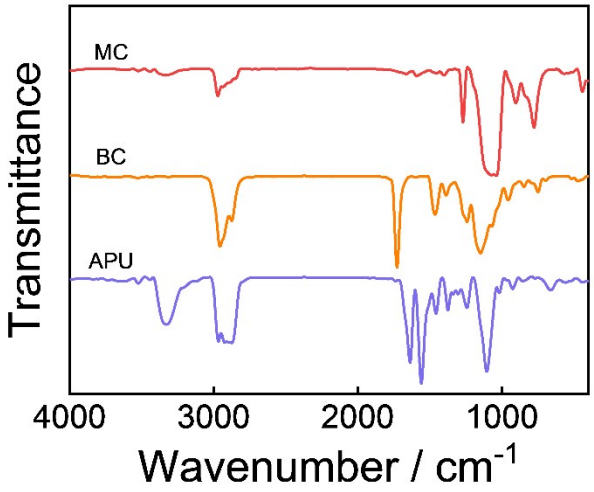


**Fig. S5.** FTIR spectra of raw materials of IAE (MC, BC, and APU).

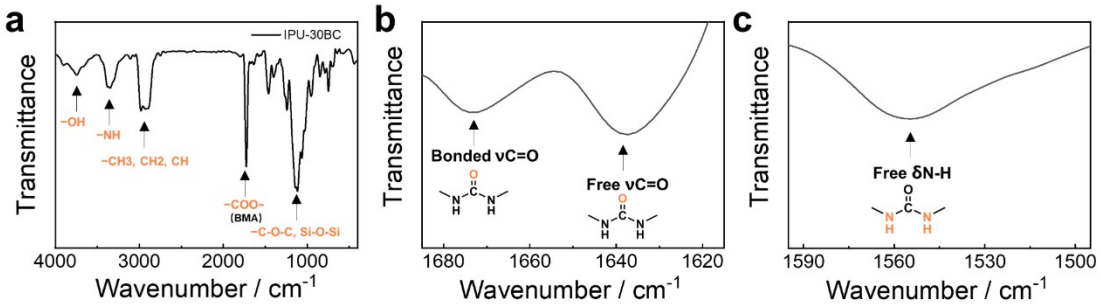


**Fig. S6.** FTIR spectra of IPU-30BC. (a) The peak of hydroxyl at 3600cm$^{-1}$ appeared to verify the successful preparation of IPU-30BC; (b) The local magnification of the characteristic peaks of C=O; (c) The local magnification of the characteristic peaks of N−H.

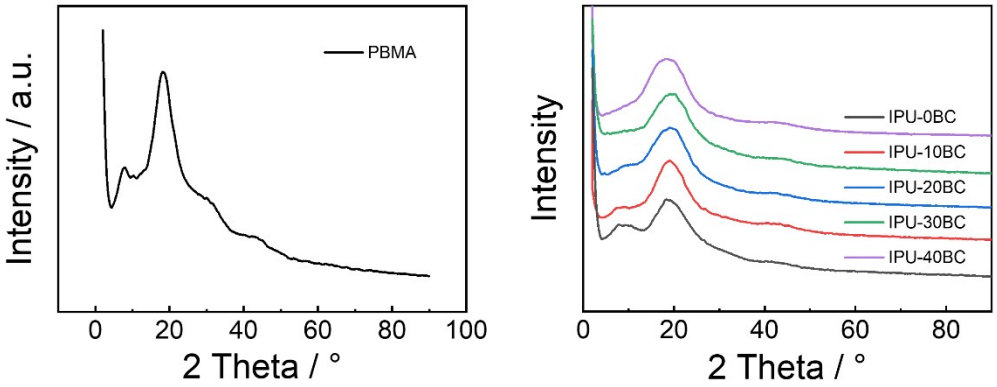


**Fig. S7.** XRD curves of PBMA and IPU-xBC.

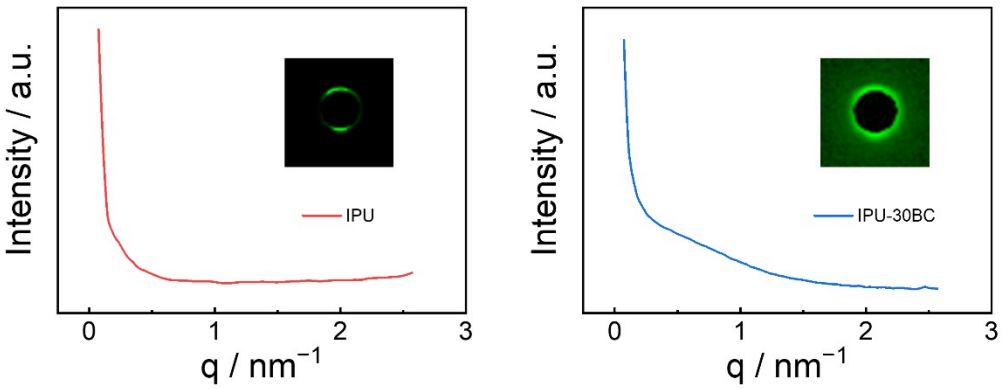


**Fig. S8.** SAXS profiles of IPU and IPU-30BC.

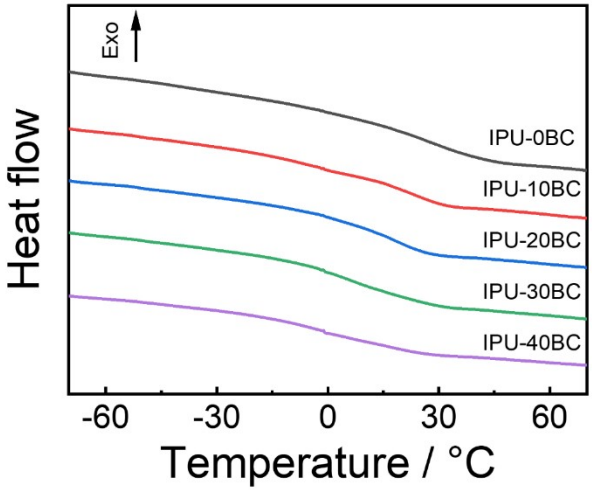


**Fig. S9.** DSC curves of IPU-xBC.

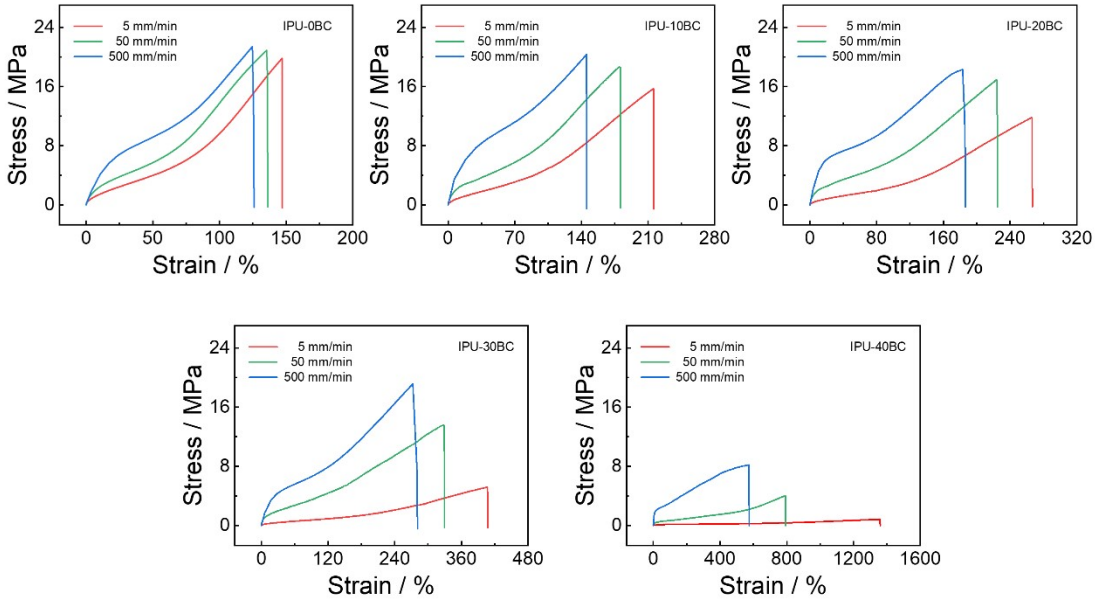


**Fig. S10.** Stress–strain curves of IPU-xBC at a rate of 5 mm·min$^{-1}$, 50 mm·min$^{-1}$, and 500 mm·min$^{-1}$. The elastomers with higher BC content exhibited more pronounced changes in their elastic moduli.

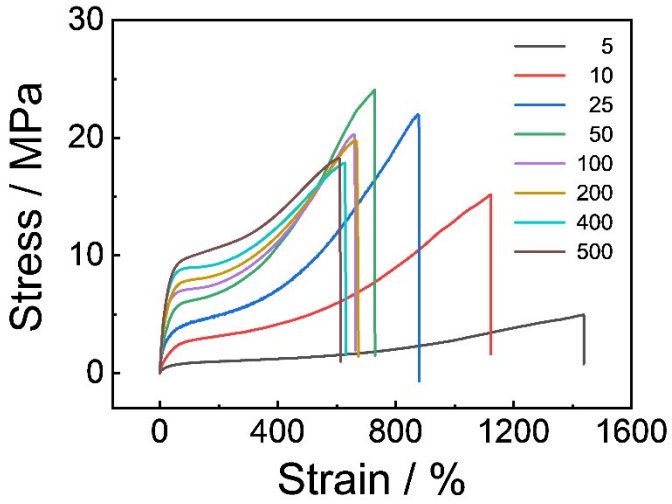


**Fig. S11.** Stress–strain curves of the IPU at different strain rate. The elastic moduli just increased rapidly from 5 mm·min$^{-1}$ to 50 mm·mm$^{-1}$, stagnant growth was observed when the strain rate exceeded 50 mm·min$^{-1}$.

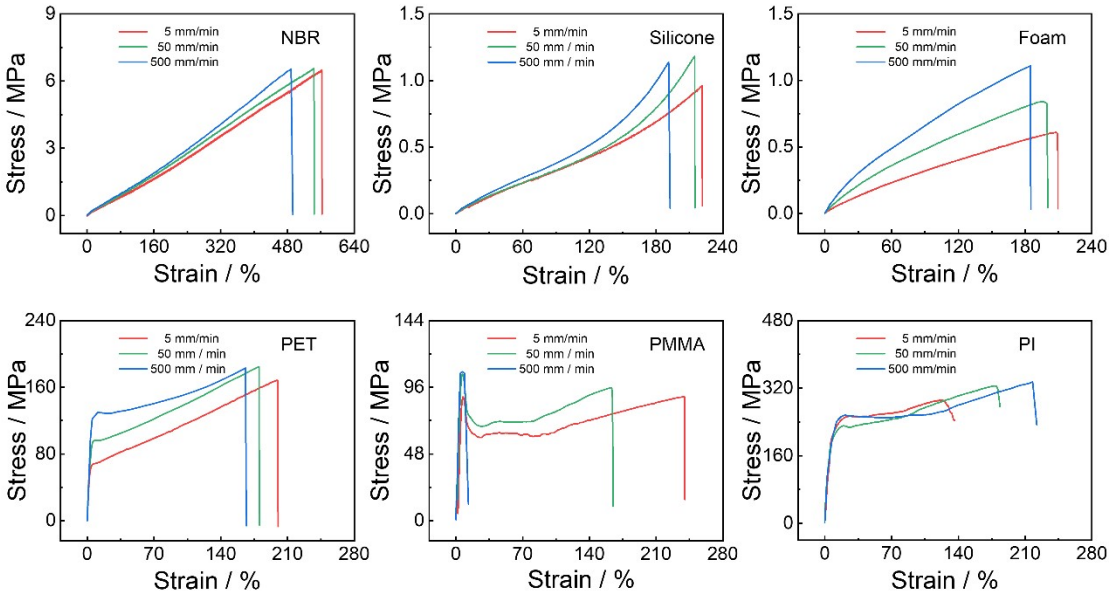


**Fig. S12.** Stress–strain curves of common soft materials (NBR, Silicone, Foam) and rigid materials (PET, PMMA, PI) at different strain rate. No correlation was observed between their elastic moduli and the strain rate.

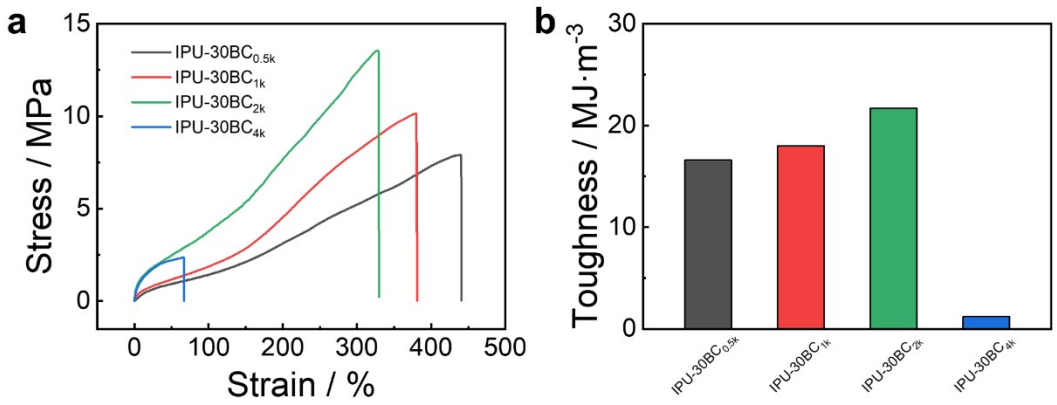


**Fig. S13.** The mechaincal properties of IAEs with varying chain lengths of PBMA. (a) Stress−strain curves; (b) Fracture energy.

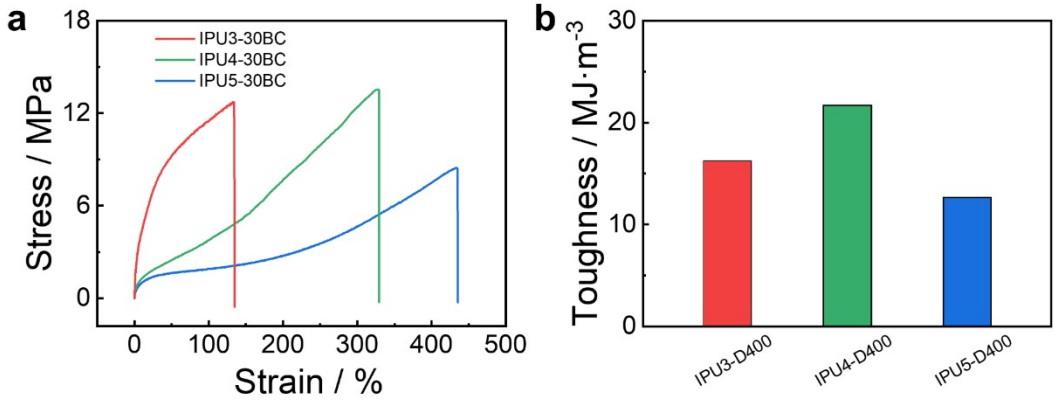


**Fig. S14.** The mechaincal properties of IAEs with different relative ratios of isocyanate and polyetheramine in polyurea. (a) Stress–strain curves; (b) Fracture energy.

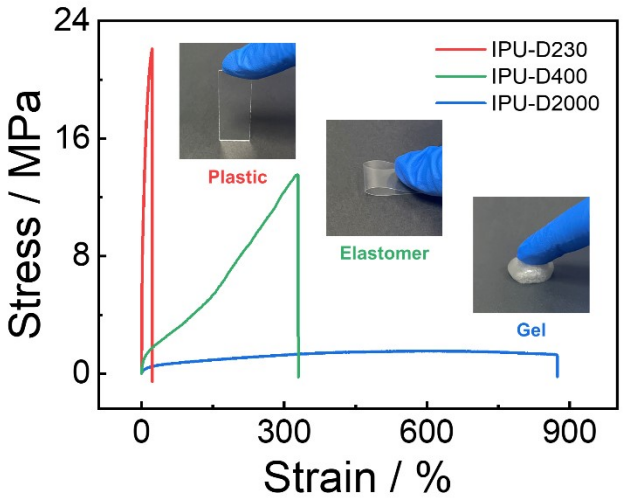


**Fig. S15.** Stress–strain curves and morphological form of the IAEs with different polyetheramine in polyurea chain. These samples displayed markedly divergent mechanical properties and manifested plastic, elastomer, and gel characteristics.

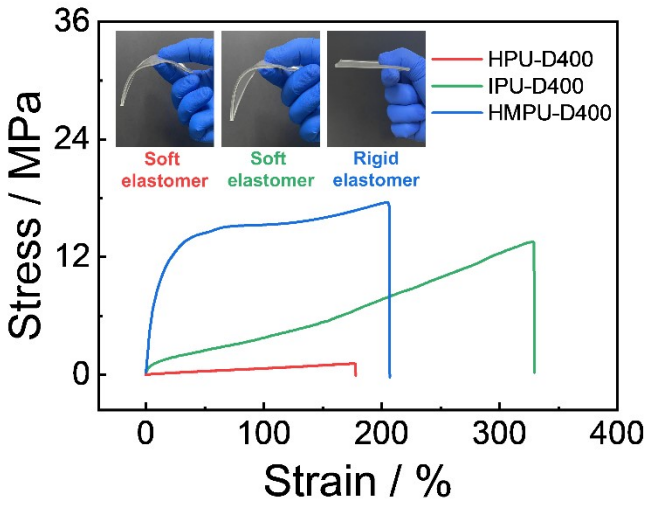


**Fig. S16.** Stress–strain curves and morphological form of the IAEs with different isocyanate in polyurea chain. The IAE with HDI or IPDI was a soft elastomer which has the relatively low elastic modulus, while the IAE with HMDI was a rigid elastomer because of its high elastic moduli.

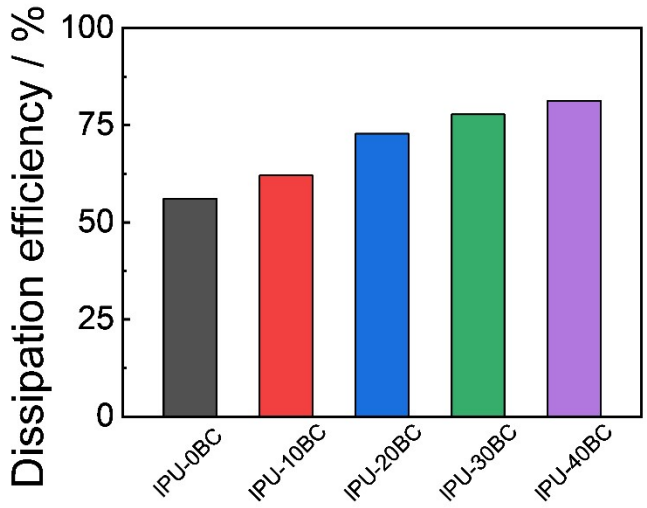


**Fig. S17.** The dissipation efficiency of IPU-xBC. The dissipation efficiency of IAEs increase as the BC content.

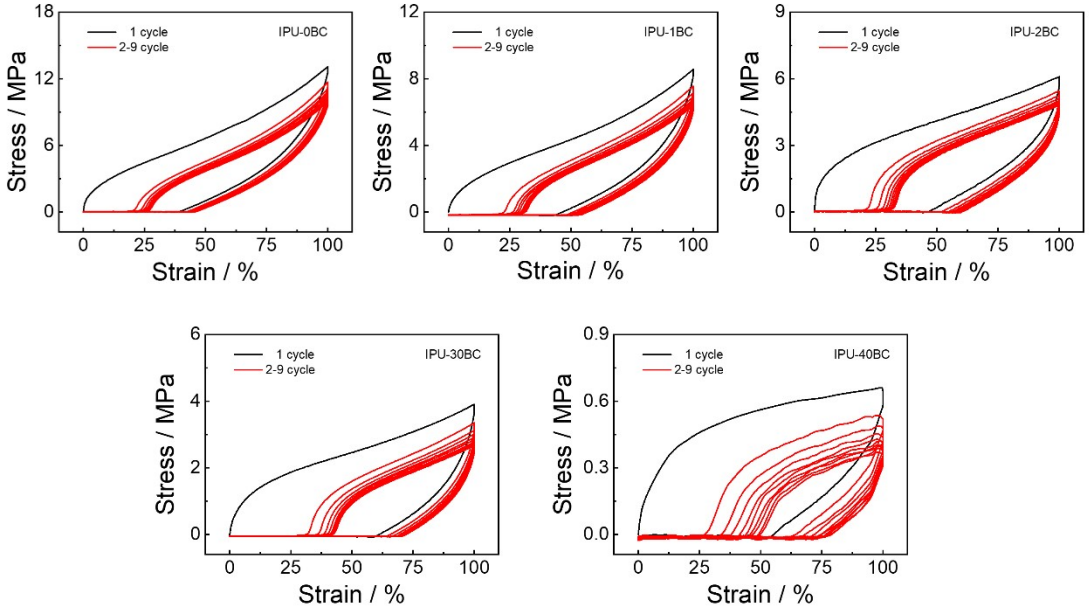


**Fig. S18.** Ten consecutive cyclic tensile curves of IPU-xBC at 100% strain.

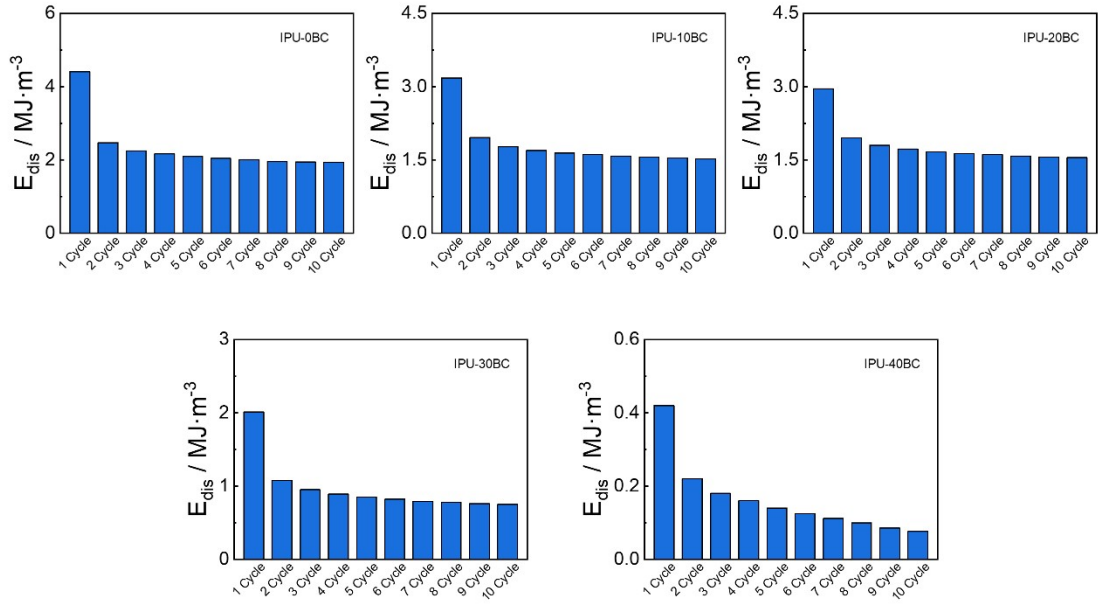


**Fig. S19.** The stability of IPU-xBC in consecutive cyclic tensile. Hysteresis loops for all elastomers stabilized after five cyclic tensile tests, with the exception of IPU-40BC, which exhibited significant fluctuations in hysteresis loop areas during each cycle.

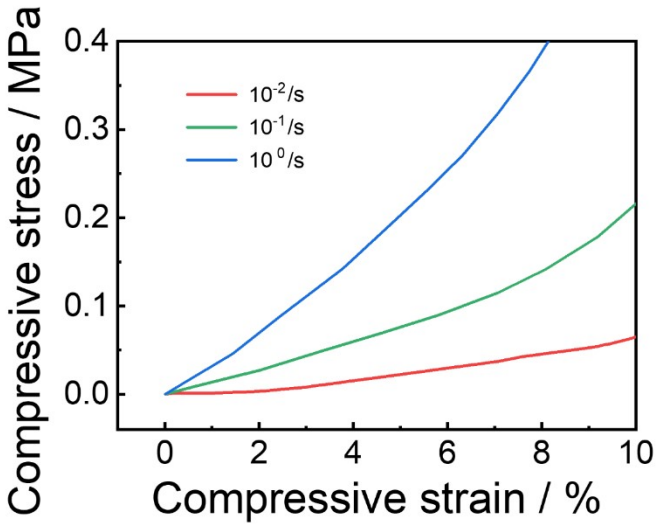


**Fig. S20.** Compression data for IPU-30BC at different strain rates.

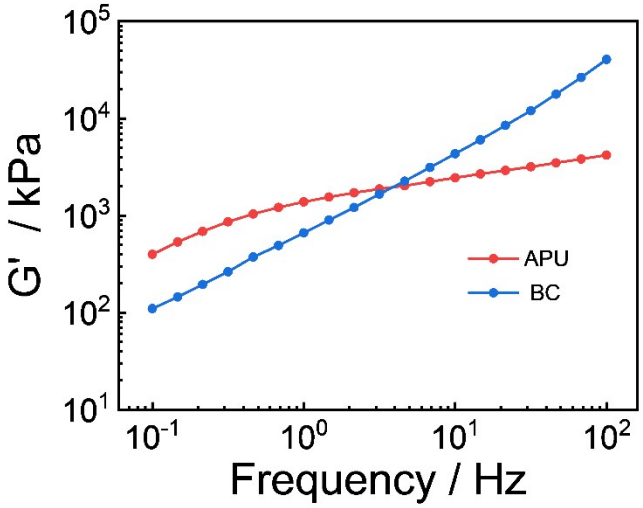


**Fig. S21.** Rheology curve of APU and BC. The rheological curve of BC exhibited a more evident frequency dependence compared to that of APU.

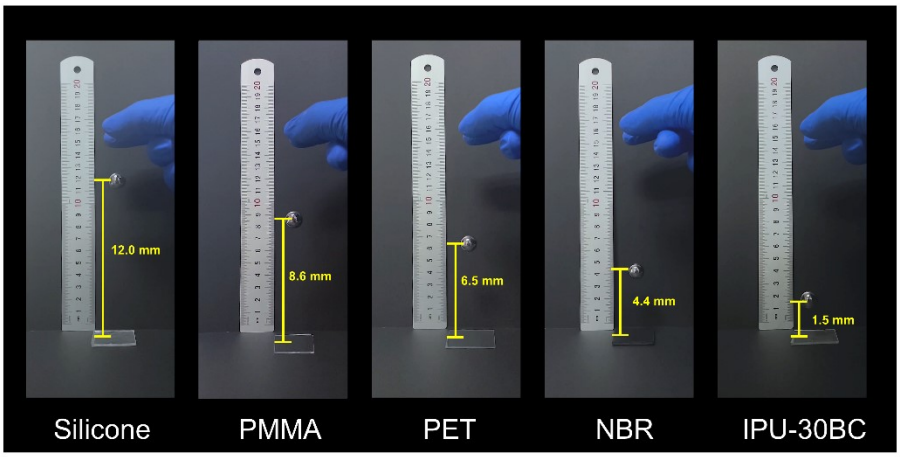


**Fig. S22.** Photographs showing the different rebound heights of a steel ball which dropped at the height of 20 cm on IPU-30BC and common materials. The rebound height of the IPU-30BC is the lowest compared to other typical materials.

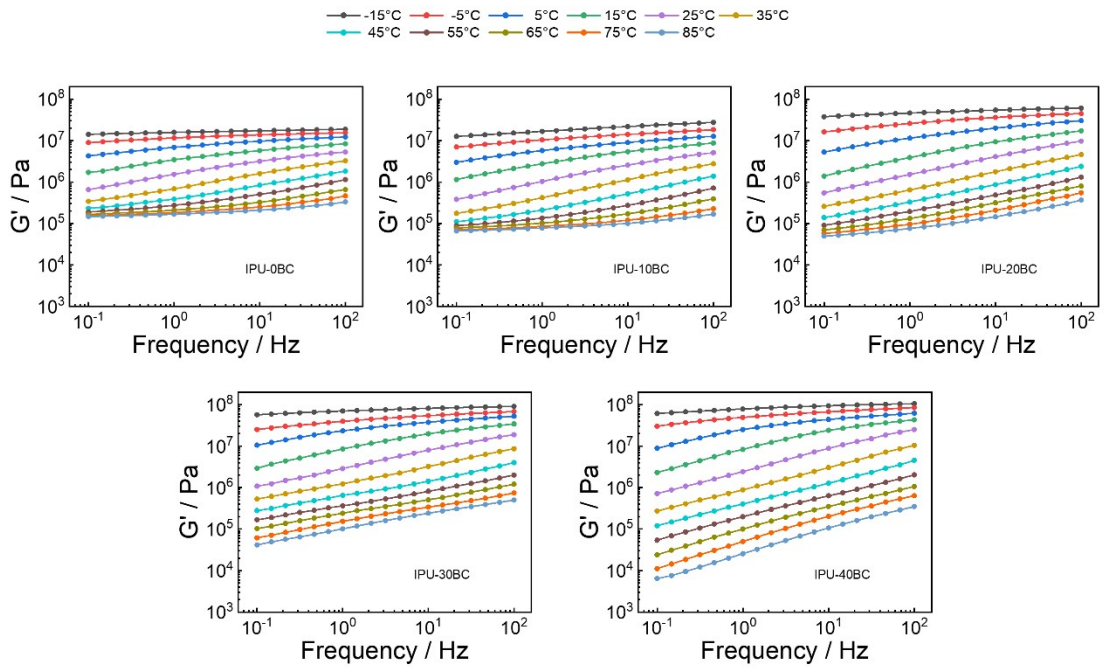


**Fig. S23.** Rheology curve of IPU-xBC in different temperature. G′ data of IPU-30BC over a $10^{-1} - 10^{2}$ Hz frequency range and a −15°C ~ 85 °C temperature range.

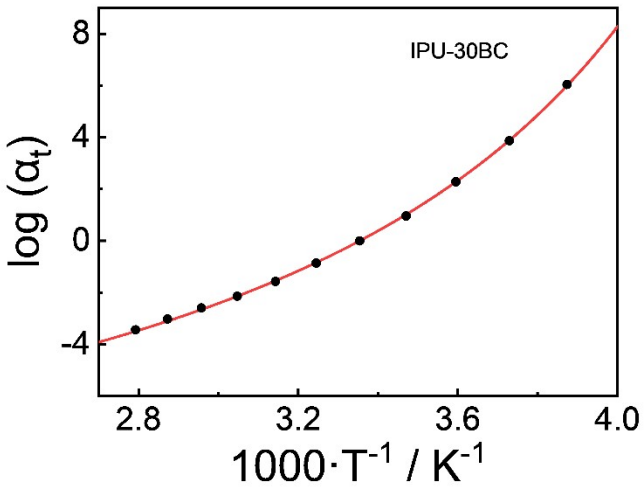


$$\log(\alpha_t) = \frac{C_1(T - T_f)}{C_2 + (T - T_f)}$$

$T_f = 25°C$

$T_f = 5°C \;\; \log(\alpha_t) = 2.28$

$T_f = 45°C \;\; \log(\alpha_t) = -1.57$

$C_1 = 9.53, \;\; C_2 = 103.59$

$$\log(\alpha_t) = \frac{-9.53(T - T_f)}{103.59 + (T - T_f)}$$

**Fig. S24.** Shift factors ($\alpha_t$) of the IPU-30BC.

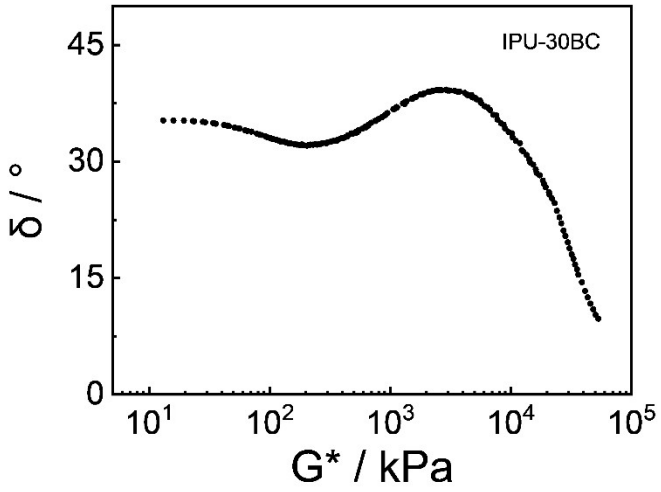


**Fig. S25.** Van-Gurp-Palmen plots of IPU-30BC. The plot of IPU-30BC is continuous, which indicates that TTS holds.

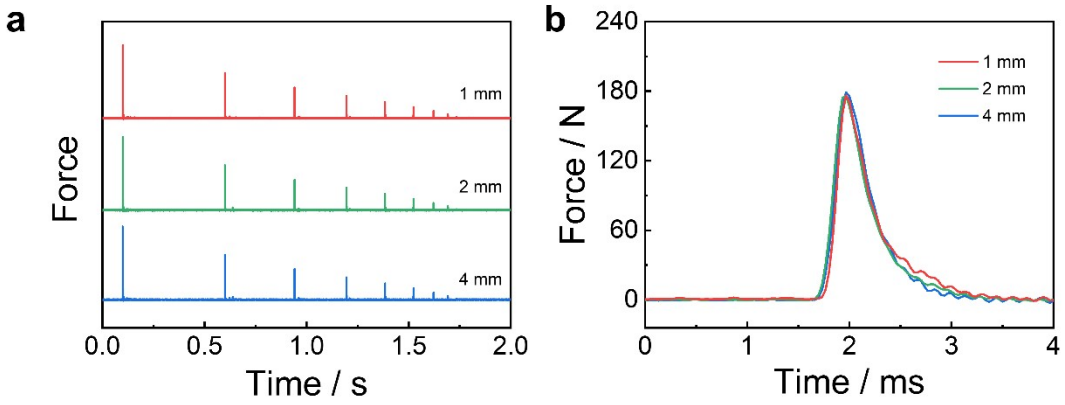


**Fig. S26.** The falling-ball impact for PMMA with different thicknesses. (a) Force–time curves for PMMA; (b) The magnified view of maximum transient force.

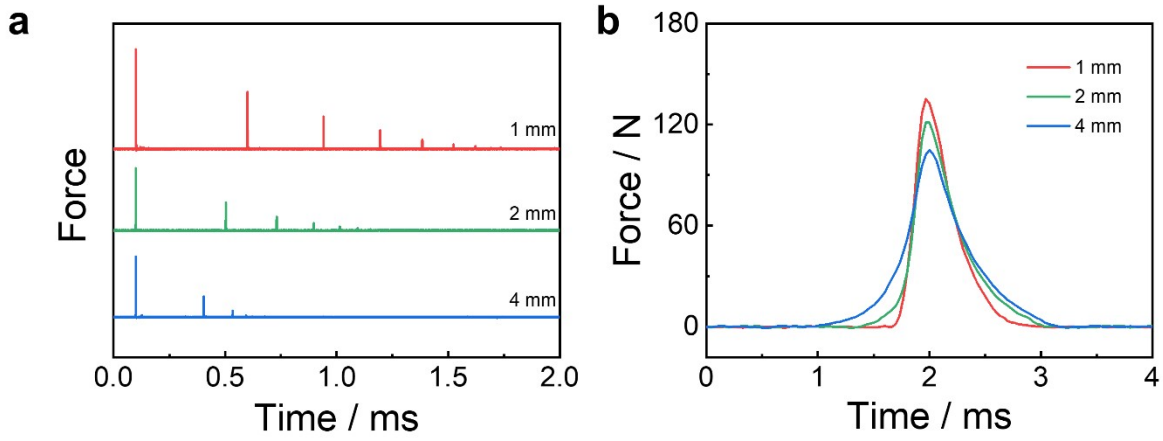


**Fig. S27.** The falling-ball impact for NBR with different thicknesses. (a) Force–time curves for NBR; (b) The magnified view of maximum transient force.

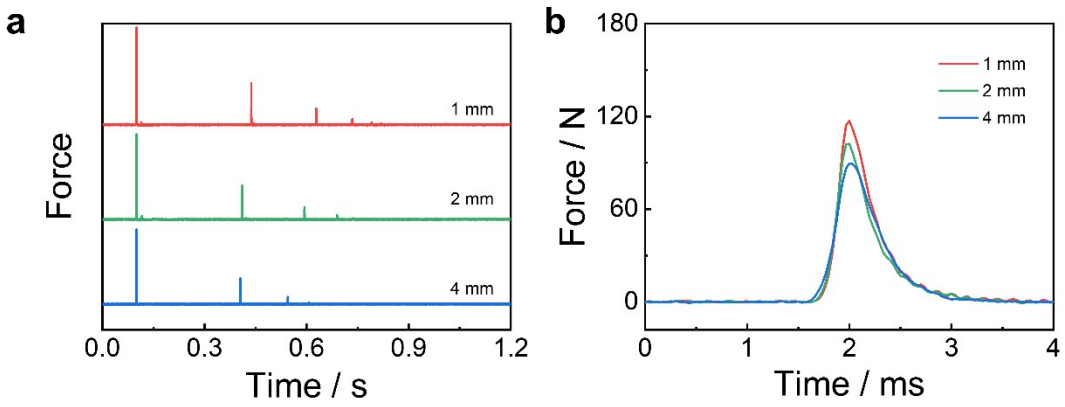


**Fig. S28.** The falling-ball impact for NBR with different thicknesses. (a) Force–time curves for IPU-30BC; (b) The magnified view of maximum transient force.

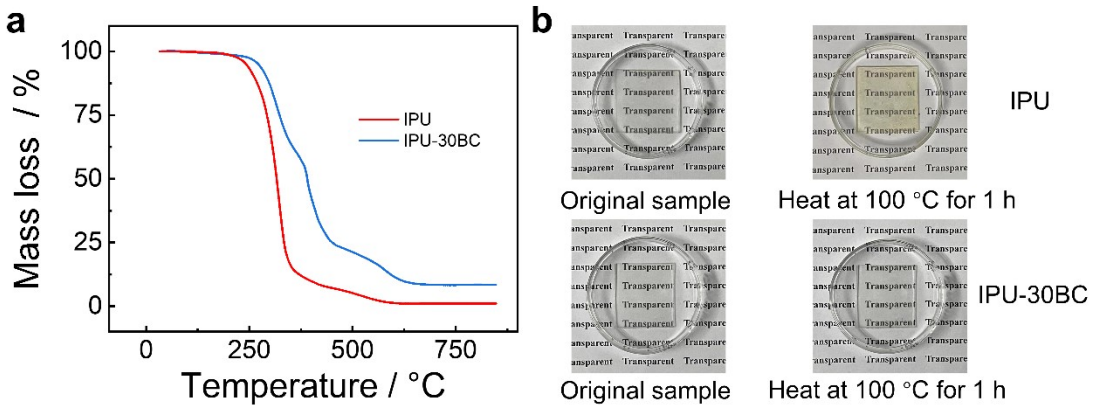


**Fig. S29.** Thermal stability of IPU-30BC and IPU. (a) Thermal decomposition curve of IPU and IPU-30BC; (b) Transparent IPU turns yellow after heated at 100 °C, while transparent IPU-30BC remain stable after heated at 100 °C.

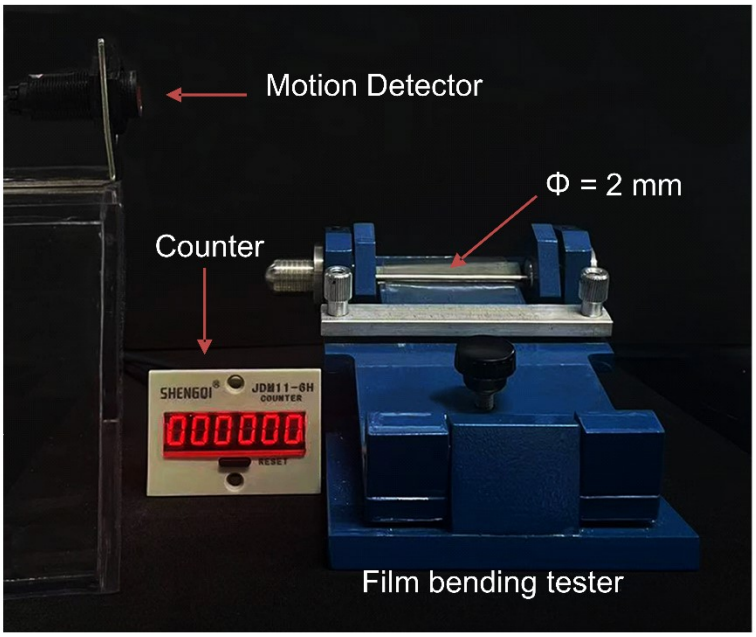


**Fig. S30.** Film bending tester to examine the flexibility of coatings.

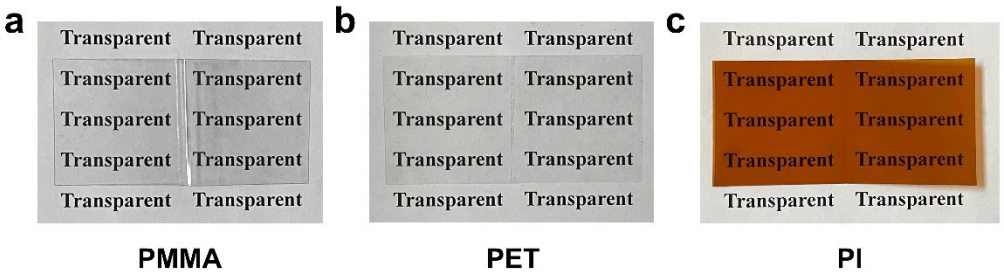


**Fig. S31.** The flexibility of PMMA, PET, and PI. Photographs showing the crease of the 1-mm-thick PMMA, PET and PI coatings after bent to a U shape with an inner diameter of 2 mm by film bending tester.

**Fig. S32.** Photographs showing the IPU-30BC can be used as a film for folding screen phones.


**Fig. S33.** The protective ability of IPU-30BC and common rigid materials. (a) A needle-shaped impactor fell from a height of 50 cm, The IPU-30BC and other rigid coatings can protect the phone from puncture; (b) A 33g ball fell from a height of 30 cm and hit the phone, only IPU-30BC can protect it.

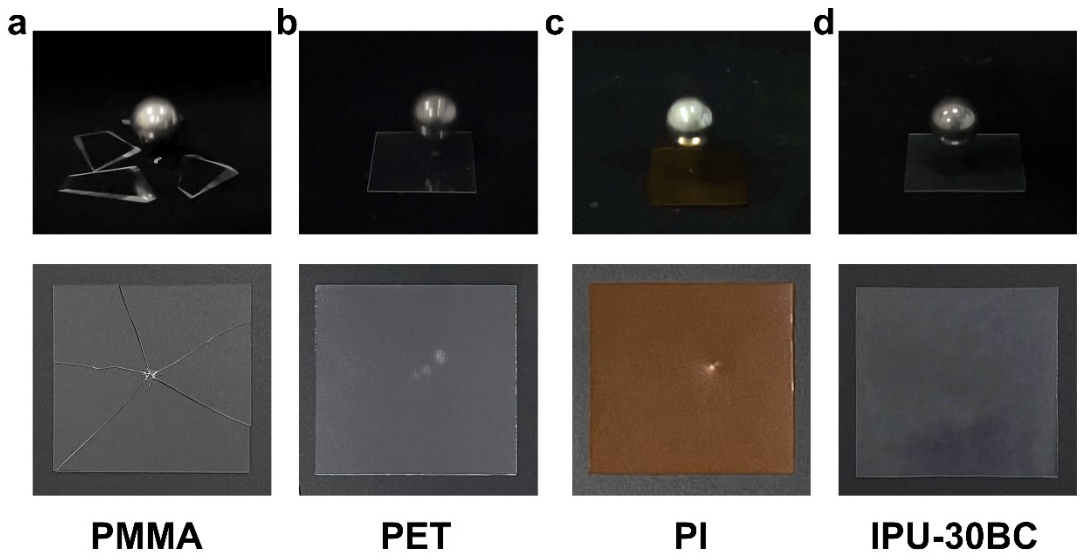


**Fig. S34.** The damage degree of coatings after being impacted by a steel ball dropped at the height of 50 cm. (a) PMMA; (b) PET; (c) PI; (d) IPU-30BC.

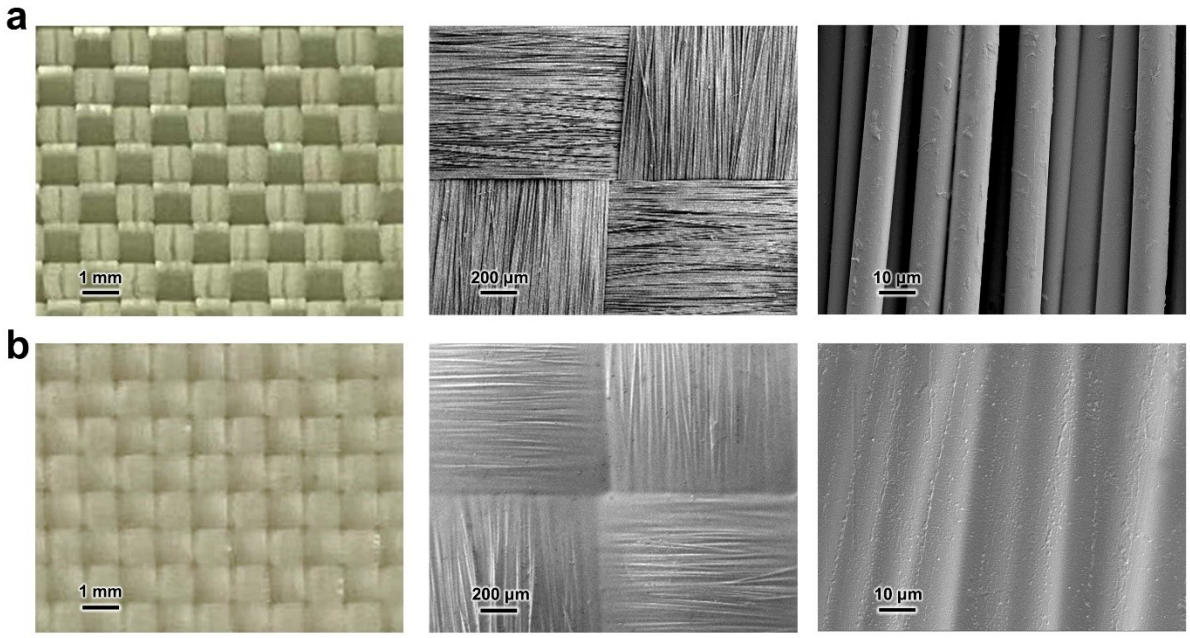


**Fig. S35.** Changes in the microscopic morphology of Kevlar fabrics after dip coating treatment. (a) SEM images of Kevlar; (b) SEM images of composite fabric prepared by IPU-30BC and Kevlar.

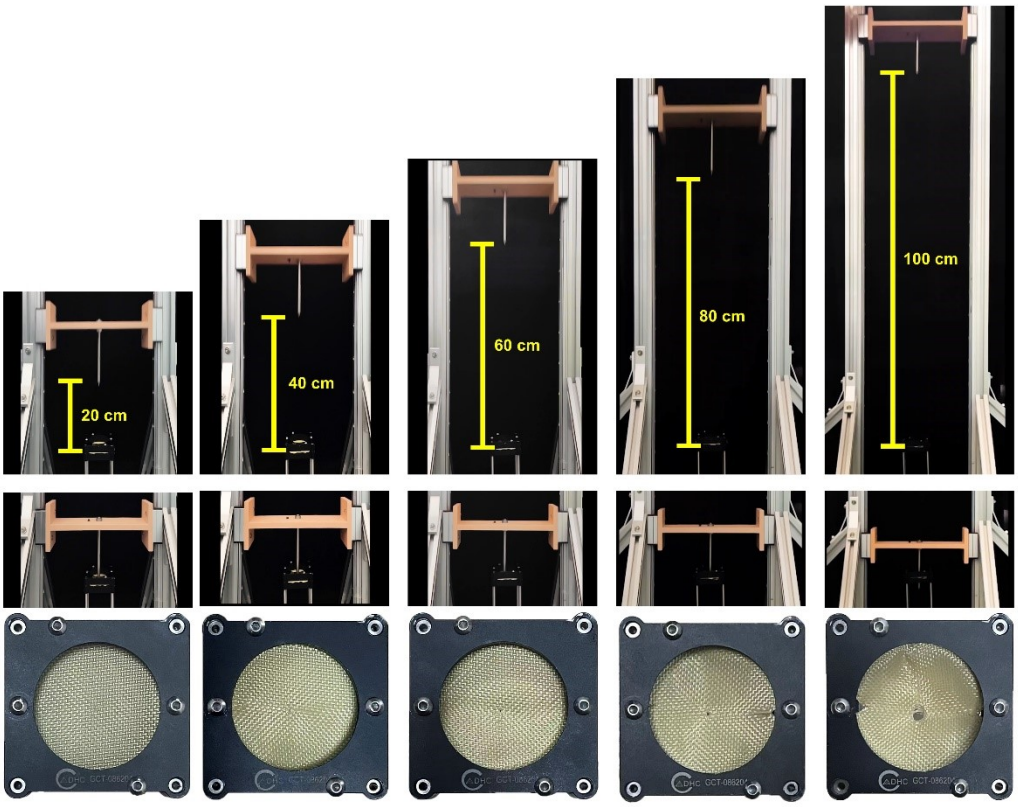


**Fig. S36.** The damage degree of the one-layer composite fabrics prepared by IPU-30BC and Kevlar after impactor dropped in different height (20 cm, 40 cm, 60 cm, 80 cm, and 100 cm). Penetration of the composite fabric occurred only when the falling height of the impactor exceeded 80 cm.

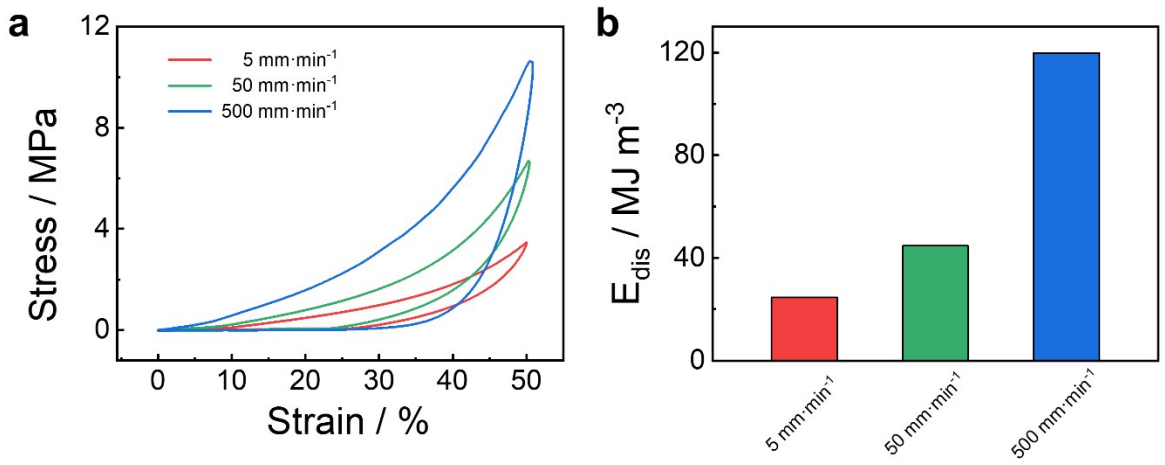


**Fig. S37.** Cyclic compression test in different strain rates. (a) Compression stress-strain curves of IPU-30BC at a rate of 5 mm·min$^{-1}$, 50 mm·min$^{-1}$, and 500 mm·min$^{-1}$; (b) The energy dissipation of IPU-30BC in different strain rate.

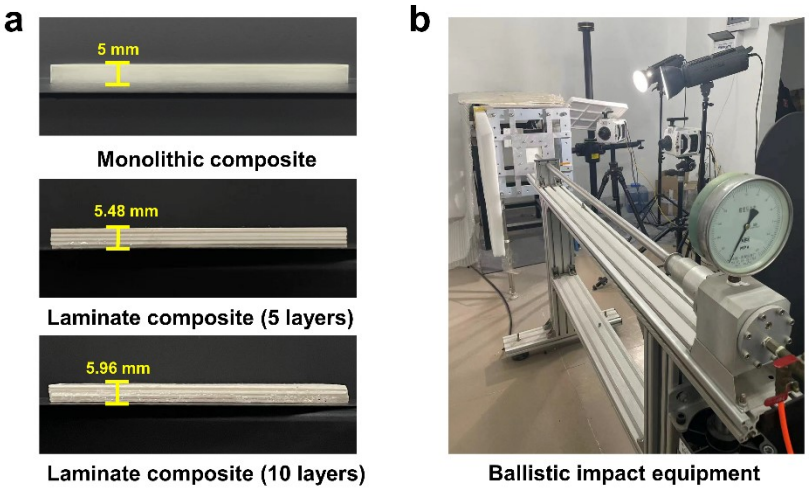


**Fig. S38.** The ballistic impact test for composite prepared by IPU-30BC and ceramic. (a) The monolithic composite and laminate composite prepared by IPU-30BC and ceramic with the thickness of 5 mm, 1 mm, and 0.5 mm. (b) The air gun and high-speed camera used for the ballistic impact equipment.

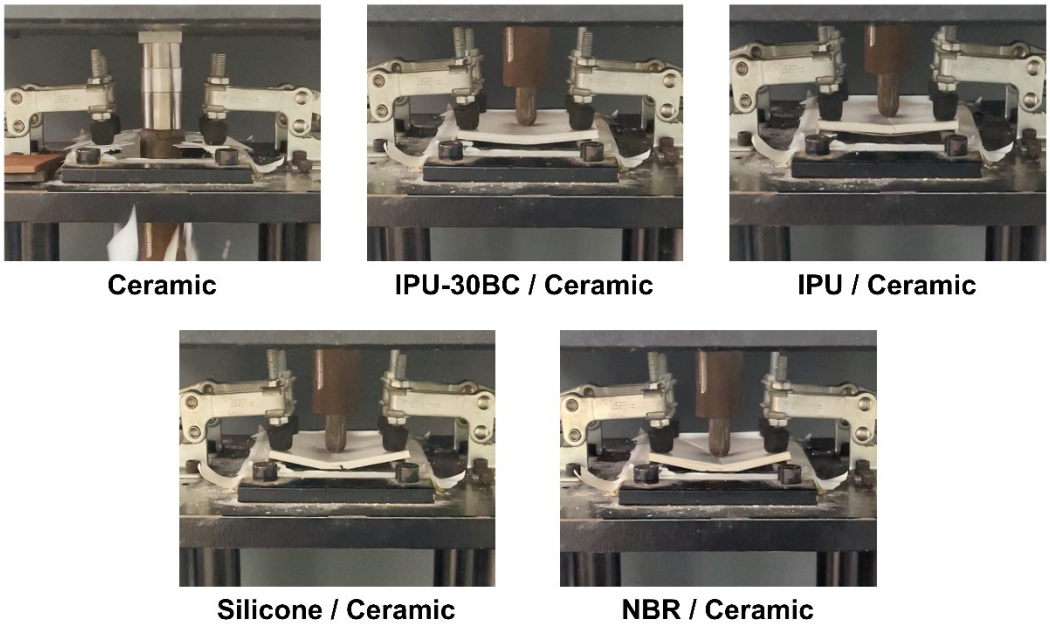


**Fig. S39.** The damage degree of composite ceramic with different cushion layers in the drop-hammer impact test. The composite with IPC-30BC suffered the least damage compared to IPU, RTV silicone, and NBR.

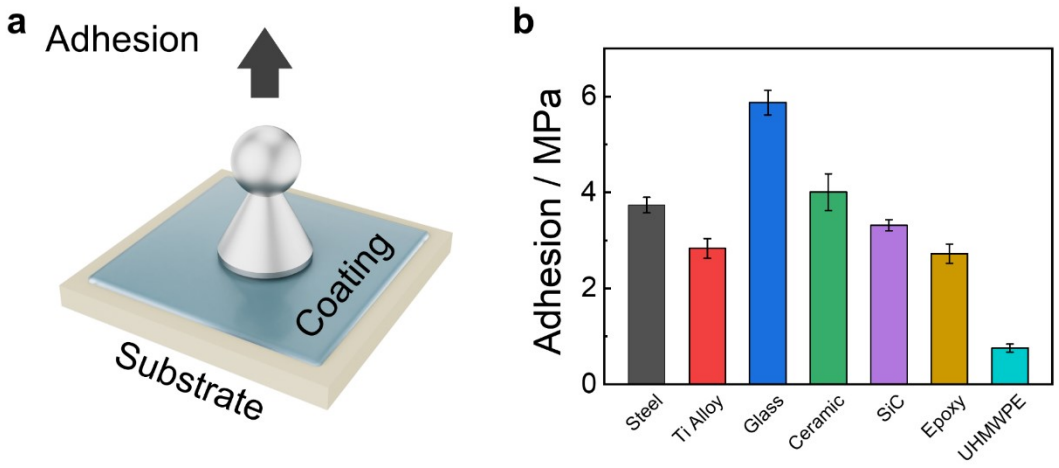


**Fig. S40.** The adhesion tests of IPU-30BC in different substrates. (a) The methods employed for the adhesion tests; (b) Adhesion strength of IPU-30BC to various substrates.

**Table S1.** The mechanical strength of IAEs with different BC content at different strain rates.

| Sample | Toughness /MJ·m$^{-3}$ | Elastic moduli / MPa | | |
|---|---|---|---|---|
| | | 5 mm·min$^{-1}$ | 50 mm·min$^{-1}$ | 500 mm·min$^{-1}$ |
| IPU-0BC | 12.7 | 21.6 | 28.3 | 39.1 |
| IPU-10BC | 15.6 | 12.7 | 25.1 | 40.6 |
| IPU-20BC | 17.8 | 8.7 | 24.3 | 41.2 |
| IPU-30BC | 21.7 | 3.5 | 17.3 | 40.7 |
| IPU-40BC | 13.5 | 2.2 | 8.6 | 34.3 |

**Table S2.** Initial ingredients of IAEs with varying chain lengths of PBMA in BC and their mechanical strength at different strain rates.

| Sample | MC /g | BC[a] /g | APU[a] /g | Elastic moduli / MPa | | |
|---|---|---|---|---|---|---|
| | | | | 5 mm·min$^{-1}$ | 50 mm·min$^{-1}$ | 500 mm·min$^{-1}$ |
| IPU-30BC$_{0.5k}$ | 1 | 3 (BC$_{0.5k}$) | 6 | 2.4 | 5.6 | 10.4 |
| IPU-30BC$_{1k}$ | 1 | 3 (BC$_{1k}$) | 6 | 2.5 | 8.6 | 22.1 |
| IPU-30BC$_{2k}$ | 1 | 3 (BC$_{2k}$) | 6 | 3.5 | 17.3 | 40.7 |
| IPU-30BC$_{4k}$ | 1 | 3 (BC$_{4k}$) | 6 | 8.3 | 18.5 | 27.9 |

[a] BC$_x$ was an epoxy–oligosiloxane nanocluster with hyperbranched PBMA, where the x represent the molecular weight of PBMA.

[b] APU was an amino-terminated polyurea prepared by isocyanate (IPDI) and polyetheramine (D400) in a ratio of 4:5.

**Table S3.** Initial ingredients of IAEs with different relative ratios of isocyanate and polyetheramine in polyurea and their mechanical strength at 50 mm·min$^{-1}$.

| Sample | MC /g | BC[a] /g | APU[b] /g | Stress /MPa | Strain /% | Elastic moduli /MPa |
|---|---|---|---|---|---|---|
| IPU3-30BC | 1 | 3 | 6 (3 IPDI-4 D400) | 12.7 | 132 | 63.7 |
| IPU4-30BC | 1 | 3 | 6 (4 IPDI-5 D400) | 13.5 | 329 | 17.3 |
| IPU5-30BC | 1 | 3 | 6 (5 IPDI-6 D400) | 8.4 | 434 | 14.5 |

[a] BC in this group was an epoxy–oligosiloxane nanocluster with PBMA of 2000 molecular weight.

[b] APU (x IPDI-y D400) was an amino-terminated polyurea prepared by isocyanate (IPDI) and polyetheramine (D400) in a ratio of x:y.

**Table S4.** Initial ingredients of IAEs with different isocyanate or polyetheramine in polyurea and their mechanical strength at 50 mm·min$^{-1}$.

| Sample | MC /g | BC[a] /g | APU[b] /g | Stress /MPa | Strain /% | Elastic moduli /MPa |
|---|---|---|---|---|---|---|
| IPU-D230 | 1 | 3 | 6 (4 IPDI-5 D230) | 22.1 | 22 | 281.1 |
| IPU-D2000 | 1 | 3 | 6 (4 IPDI-5 D2000) | 1.2 | 874 | 5.48 |
| HPU-D400 | 1 | 3 | 6 (4 HDI-5 D400) | 1.1 | 177 | 0.65 |
| HMPU- D400 | 1 | 3 | 6 (4 HMDI-5 D400) | 12.4 | 205 | 125 |

[a] BC in this group was an epoxy–oligosiloxane nanocluster with PBMA of 2000 molecular weight.

[b] APU (4 isocyanate -5 polyetheramine) was an amino-terminated polyurea prepared by different kinds of isocyanate and polyetheramine in a ratio of 4:5.

**Table S5.** The number of layers for fabric to fully resist the puncture.

| Sample | 20 cm | 40 cm | 60 cm | 80 cm | 100 cm |
|---|---|---|---|---|---|
| Kevlar | 4 | 5 | 7 | 9 | 11 |
| PBS/Kevlar | 3 | 4 | 5 | 5 | 6 |
| IPU-30BC/Kevlar | 1 | 1 | 1 | 1 | 2 |

**Table S6.** The characterization of Kevlar and its composite (200 mm × 200 mm).

| Sample | Weight / g | Thickness / mm |
|---|---|---|
| Kevlar | 0.300 | 20.4 |
| PBS/Kevlar | 0.317 | 21.8 |
| IPU-30BC/Kevlar | 0.321 | 22.1 |

**Table S7.** The characterization of Ceramic and its composite (100 mm × 100 mm).

| Sample | layer | Weight / g | Thickness / mm |
|---|---|---|---|
| Monolithic composite (IPU-30BC) | 1 | 180.2 | 5 |
| Laminated composite (IPU-30BC) | 5 | 182.3 | 5.48 |
| Laminated composite (IPU-30BC) | 10 | 188.4 | 5.96 |
| Laminated composite (IPU) | 10 | 190.1 | 6.03 |
| Laminated composite (Silicone) | 10 | 186.3 | 6.01 |
| Laminated composite (NBR) | 10 | 184.2 | 5.89 |

**Table S8.** Material parameters for fabric used PLASTIC_KINEMATIC model.

| Material | RO/ kg/m$^3$ | E/ GPa | PR | SIGY /MPa | ETAN /MPa | SRC | SPR | BEAT | FS % | VP |
|---|---|---|---|---|---|---|---|---|---|---|
| Kevlar | 1.4 | 120 | 0.3 | 1000 | 10000 | 0 | 0 | 1 | 15 | 0 |

**Table S9.** Material parameters for steel ball used MAT_RIGID model.

| Material | RO/ kg/m$^3$ | E/ GPa | PR | N | M | COUPLE | ALIAS |
|---|---|---|---|---|---|---|---|
| Steel ball | 7.85 | 200 | 0.3 | 0 | 0 | 0 | 0 |

**Table S10.** Material parameters for coating used MAT_ELASTIC model.

| Material | RO/ kg/m$^3$ | E/ GPa | PR | DA | DB |
|---|---|---|---|---|---|
| Coating (PBS) | 1.1 | 0.1 | 0.5 | 0 | 0 |
| Coating (IPU-30BC) | 1.08 | 3.6 | 0.5 | 0 | 0 |

**References**


1 R. Chen, Q. Xie, H. Zeng, C. Ma and G. Zhang, *J. Mater. Chem. A.* 2020, **8**, 380−387.

2 R. H. Ewoldt, P. Winter, J. Maxey and G. H. Mckinley, *Rheol. Acta.* 2010, **49**, 191–212.

3 ASTM D4541-22. Standard Test Method for Pull-off Strength of Coatings Using Portable Adhesion Testers; ASTM International: West Conshohocken, PA, 2022.

4 X. Zhang, K. Wu, Y. Ni and L. He, *Nat. Commun.* 2022, **13**, 7719.

5 C. Xu, Y. Wang, J. Wu, S. Song, S. Cao, S. Xuan, W. Jiang and X. Gong, *Compos. Sci. Technol.* 2017, **153**, 168−177.

6 NIJ Standard 0101.06**.** Resistance of Personal Body Armor; National Institute of Standards and Technology, United States of America, 2008.

7 MIL-DTL-46593B. Projectile, Calibers .22, .30, .50, and 20 mm Fragment-Simulating; Military Detail, United States of America, 2023.

8 Y. Wang, S. Wang, C. Xu, S. Xuan, W. Jiang and X. Gong, *Compos. Sci. Technol.* 2016, **127**, 169−176.

9 S. Cao, H. Pang, C. Zhao, S. Xuan and X. Gong, *Compos. B. Eng.* 2020, **185**, 107793.